Corrosion of aluminium in ordinary Portland cement paste: influence of matrix porosity and the presence of $LiNO_3$ corrosion inhibitor

Running head: Aluminium corrosion in OPC: Influence of $LiNO_3$ and porosity

Sebastien Caes*, Alfred Christopher Gurning, Xiang Li, Valdir de Souza, Bruno Kursten

SCK CEN, Belgian Nuclear Research Center, Boeretang 200, Mol, Belgium

* sebastien.caes@sckcen.be

Keywords

Aluminium; anaerobic corrosion; $LiNO_3$; mass transfer limitation; Ordinary Portland Cement

Abstract

The Belgian reactor 1 fuel cladding is made of aluminium. If disposed in a geological disposal repository, aluminium could come into contact with Ordinary Portland Cement, and is going to corrode to form hydrogen gas and aluminium hydroxide. In this study, the long term corrosion was evaluated by Electrochemical Impedance Spectroscopy on metal embedded in cement paste immersed in saturated calcium hydroxide solution under anaerobic conditions. Mass transfer effects were investigated by embedding aluminium in cement paste with two different porosities. $LiNO_3$ was also added to the systems to study its corrosion inhibiting effect. After high initial values, the corrosion rate rapidly declined to reach a steady state after a few days. After ~100 days, the corrosion rate was the lowest when cement paste possessing a low porosity with the addition of $LiNO_3$ was used and the highest when cement paste with high porosity without $LiNO_3$ was used. Finally, SEM-EDS revealed that the corrosion product layer was thicker than expected by EIS measurements, while it is only composed of aluminium and

oxygen. Aluminium was found to diffuse into the cement paste close to this corrosion product layer.

1. Introduction

The Belgian Research Reactor 1 (BR1) is an air-cooled graphite-moderated reactor. Initially, it is used for the production of radio-isotopes and for the research into reactor and neutron physics. At present, it is mainly being used for training of nuclear experts, for calibration of measuring instruments and for irradiation of components. The fuel rods of the BR1 are made of natural unalloyed metallic uranium, coated with an aluminosilicate alloy bonding layer and an $U(Al,Si)_3$ anti-diffusion layer, which is encapsulated in an aluminium container [1]. Metallic aluminium was chosen as fuel cladding because it possesses a high thermal conductivity, a low thermal neutron capture cross section and good oxidation resistance and mechanical properties [2].

One potential solution for the long term management of this fuel, which will eventually become waste, is geological disposal. To do so, a direct embedding of the waste in a cement-based matrix is envisaged, bringing metallic aluminium in contact with the cement paste. Ordinary Portland Cement (OPC) is one of the most widely used materials for conditioning radioactive wastes because it is inexpensive, it can easily be supplied, and it exhibits high stability over time after hydration [3]. However, OPC possesses a high pH pore water solution. The oxide layer formed on the aluminium surface is amphoteric and therefore not resistant to corrosion when brought in contact with the highly alkaline cement pore water because the protected oxide film dissolves to form e.g. aluminium oxides and hydroxides, with the liberation of hydrogen gas (in anaerobic conditions) [4-9]. As a consequence of this phenomenon, the corrosion products will take up a larger volume compared to the original metal, leading to an increase of

the internal stresses and damages of the matrix [9,10]. To decrease these problems, different methods can be used. First, lowering the pH of the cement pore water and/or reducing available free water reduces the reaction of aluminium in the cement matrix [11]. It is reported in the literature that the corrosion of Al is significantly reduced when cement pastes with a lower pH (compared to OPC) were used, such as e.g. 9:1 Blast Furnace Slag (BFS)-OPC system [10], cement with excess sulphate [11-14], or magnesium phosphate cement (MPC) [3,15,16]. Second, the corrosion rate of aluminium can be reduced by the addition of a corrosion inhibitor to the cement. Matsuo *et al.* [17] found that the addition of $LiNO_3$ inhibits the hydrogen gas generation produced during the corrosion reaction. This inhibition was attributed to the formation of a $LiH(AlO_2)_2.5H_2O$ (Li-Al) preservation film on the aluminium surface during the solidification process of the cement-based material [18]. At least 1.5 wt.% lithium nitrate should be added to substantially decrease the corrosion rate. And, 3 wt.% $LiNO_3$, or more, is needed to reduce the hydrogen gas generation rate [19]. Due to water penetration (e.g. after breaching of the waste containers), dissolution of the protective Li-Al layer could happen. However, in a geological radioactive waste disposal, this is expected to occur when the concentration of Na_2O and K_2O, and therefore the pH of the cement pore solution, is decreased, leading to lower corrosion rates [17]. $LiNO_3$ was also used to decrease the aluminium corrosion rate in magnesium phosphate cement pastes [20], although $LiNO_3$ had a negative effect on the mechanical behaviour of this cement material.

In this paper, the long term corrosion rate of metallic aluminium embedded in OPC paste was studied. To evaluate the corrosion behaviour at long term under deep geological disposal conditions, as well as the effect of the water penetration in the cement paste after possible breaching of the waste containers, metallic aluminium embedded in OPC paste were immersed in saturated $Ca(OH)_2$ solution under anaerobic conditions one day after casting. This also allowed the curing of the cement paste. The corrosion rate was evaluated via Electrochemical

Impedance Spectroscopy (EIS). The influence of the presence of $LiNO_3$ inhibitor on the corrosion rate of metallic aluminium was also investigated. Moreover, different cement porosities, obtained by using two extreme water/cement ratios (w/c), as well as non-embedded bare aluminium, were analysed to study the influence of the mass transfer on the corrosion of aluminium. Finally, SEM-EDS analyses were carried out on cross sections of the samples to gain information on the corrosion product layer and the aluminium/cement paste interface.

2. Materials and Method

Portland cement (CEM I 52.5 N grade, Holcim) was mixed manually for 5 min with degassed milli-Q water to produce a cement paste. All preparatory work was carried out in an argon operating glove box to produce oxygen-free cement paste. Two cement pastes with two different w/c ratios (0.36 and 0.8) were used, with or without the addition of 3 wt.% $LiNO_3$. $LiNO_3$ was added to investigate its inhibiting effect on aluminium corrosion. Finally, four different cement pastes were studied:

- OPC-0.36: 0.36 w/c;
- OPC-0.36Li: 0.36 w/c + 3 wt.% $LiNO_3$;
- OPC-0.8: 0.8 w/c; and
- OPC-0.8Li: 0.8 w/c + 3 wt.% $LiNO_3$.

A pseudo three-electrode cell was used for the electrochemical measurements. The systems were composed of two aluminium electrodes (99% purity). One was considered as the working electrode, while the second one was considered as the counter and reference electrode. Both electrodes were taped with a non-conductive tape to get an exposed surface of 2.54 cm^2. The Al plates were emplaced in parallel at a distance of 0.55 cm by means of Teflon® screws. The

aluminium plates were rinsed with water and cleaned using ethanol before being embedded in a 4×4×4 cm^3 mould.

After 24 hours, the samples were demoulded and directly immersed in a saturated $Ca(OH)_2$ solution to allow the curing of the cement pastes. Degassed milli-Q water was used to prepare the $Ca(OH)_2$ solution.

The electrochemical measurements were performed using an Autolab PGSTAT 30 potentiostat combined with the NOVA 1.8 version software. EIS measurements were conducted using an excitation potential of 10 mV (peak-to-peak) in a frequency range of 10 mHz to 100 kHz, with the impedance being measured at ten frequencies per logarithmic decade. For each measurement, EIS were recorded from high to low frequencies and directly after from low to high frequencies to check for system stability. For all analysis, both measurements were similar. The EIS experimental data have been fitted with the Zview software. Polarisation measurements were recorded after EIS to obtain the value of the Tafel slopes, used for the calculation of the corrosion current by using of the Stern-Geary equation [21] and finally the corrosion rate of aluminium [22].

EIS corrosion tests were also performed by immersing bare aluminium plates into saturated $Ca(OH)_2$ solutions in anaerobic conditions (without embedding them in OPC paste) to test a system without mass transfer resistance. The same Teflon® spacers were used to separate the two aluminium plates.

To fit the EIS curves two simple Equivalent Electrical Circuits (EEC) modelling the physical properties of the studied system was used. For the system with aluminium electrodes embedded in OPC (Figure 1(a)), the EEC was composed of three parts. The first part consists of a single resistor R_{s1}, representing the solution resistance. The second part is composed of three parallel branches modelling the cement paste. One branch consists of a constant phase element

(CPE_{cem1}) representing the capacitance across the cement paste. The second branch consists of a resistor (R_{cem1}) modelling the impedance of the continuously connected micro-pores in the cement paste. The third branch is composed of a resistor (R_{cem2}) and a constant phase element (CPE_{cem2}) in series modelling the discontinuous connected micro-pores of the cement paste [3,23-25]. Finally, the last part consists of one constant phase element (CPE_{cd}) and a resistor (R_{t1}) in parallel, representing the double layer capacitance and the charge transfer resistance, respectively [3]. R_{t1} is used to calculate the corrosion rate of the aluminium in the different Al/cement systems studied in this research.

To fit the system with aluminium electrodes immersed in $Ca(OH)_2$ solution, a EEC composed of two parts was used (Figure1(b)) [26,27]. The first part consists of a resistor (R_{s2}), representing the solution resistance. The second part, which models the interface between the aluminium electrode and the solution. CPE_1 and R_c are the constant phase element and the resistance of the corrosion product film. CPE_2 is the constant phase element of the double layer and R_{t2} is the charge transfer resistance across the corrosion products precipitated on the aluminium surface. R_{t2} is used to calculate the corrosion rate of bare aluminium metal sample.

The pore size and porosity of the cement pastes were analysed by Mercury Intrusion Porosimetry (MIP; PASCAL 140/440 porosimeter). These measurements were done on the same cement pastes than the ones used for the EIS tests and aged in the same conditions, but without metallic aluminium inserted in the cement pastes. After 70 days, the cement pastes were dried for 3 days at room temperature and finally heated at 150 °C for 24 hours before to be analysed by MIP.

SEM-EDS analysis of the cross section of embedded samples was carried out with a Phenom apparatus using an accelerating voltage of 10 kV or 15 kV.

As there is no internal standard in the apparatus, EDS only provides semi-quantitative analysis.

3. Results and discussion

3.1. Mercury Intrusion Porosimetry

The porosity of the cement pastes is related to the corrosion rate of the aluminium sample. The easier the corroding solution and the elements stemming from the dissolution of the 'corrosion product layer' can diffuse through the cement paste, the higher the corrosion rate should be. One of the parameters that can affect the diffusion of saturated $Ca(OH)_2$ solution is the porosity of the cement paste, which is controlled by the w/c ratio [28].

MIP was performed on the four different OPC cement pastes used in this study (see Section 2). The main results of the MIP measurements are presented in Table 1. Even if small differences can be observed, the addition of lithium in cement does not really affect the porosity of the obtained cement pastes. The average pore radius of OPC-0.36 and OPC-0.36Li is around 10 nm, while it is around three to four times higher for OPC-0.8 (32 nm) and OPC-0.8Li (39 nm). The percentage of porosity is also around 3 times higher for OPC-0.8 and OPC-0.8Li (~30%) compared to the one of OPC-0.36 (10%) and OPC-0.36Li (7%) cement pastes.

3.2. Evolution of the corrosion rate

The difference in porosity of the cement pastes should have an effect on the corrosion rate of aluminium samples encapsulated in these matrices. Indeed, a lower porosity will limit the mass transfer through the cement paste. Therefore, a lower corrosion rate is to be expected for metallic aluminium when embedded in OPC-0.36 and OPC-0.36Li compared to OPC-0.8 and OPC-0.8Li. This hypothesis was evaluated using electrochemical techniques. EIS is a

commonly used technique to estimate the corrosion rate and behaviour of different metals, as well as for electrodes embedded in a cement paste matrix [3,15,29-33].

The evolution as a function of time of the Nyquist and Bode plots for aluminium either immersed directly in saturated $Ca(OH)_2$ solution or embedded in four different OPC cement paste matrices (described in Section 2) and then immersed in saturated $Ca(OH)_2$ solution under argon atmosphere are shown in Figure 2.

In general, the radius of the impedance semicircles observed in the Nyquist plots increased with time. This is caused by an increase of the charge transfer resistance of the corrosion process, corresponding to a decrease of the corrosion rate in function of time. For OPC-0.36, the radius of the semicircles in the Nyquist plots increased until ~30 days, after which it decreased. This coincided with the appearance of a crack in the cement paste blocks, which created a pathway for the saturated $Ca(OH)_2$ solution surrounding the cement paste to the surface of the Al sample, resulting in an increase of the corrosion rate. This crack is likely to be caused by (1) the formation of corrosion products occupying a larger volume than the metallic Al in view to its lower density and (2) the generation of hydrogen gas creating gaps in the surrounding of the metallic aluminium. Such a crack was also observed in the OPC-0.8 cement paste sample, but this time without any decrease of the radii of the Nyquist impedance semicircles. Finally, the semicircle diameters increased again until it stabilised. This could be explained by the formation of corrosion products, filling the crack and thereby limiting the contact of saturated $Ca(OH)_2$ solution with metal. It also needs to be noted that no cracks were observed when $LiNO_3$ was added to the cement paste, because of the lower corrosion rate induced by the Al/Li layer formed at the surface of the metal, but also due to the fact that in presence of nitrates, the hydrogen produced during the corrosion of aluminium chemically reacts (partially) with nitrate to form nitrite or ammonium [3], avoiding an overpressure close to the Al/cement paste interface.

Figure 3, representing the results at the end of the experiments (98-99 days) for OPC-0.36, OPC-0.36Li, OPC-0.8 and OPC-0.8Li, confirms the observation described above. For tests where $LiNO_3$ was added, larger semicircles are observed, while it is by far the largest for OPC-0.36Li. This corresponds to the lowest corrosion rate. The smallest semicircle is observed for OPC-0.8, closely followed by OPC-0.36, corresponding to the highest corrosion rate. From Figure 3, the ranking of the corrosion rate according to the environmental conditions leads to OPC-0.36Li << OPC-0.8Li < OPC-0.36 < OPC-0.8.

Figure 2 also shows that the Nyquist plots possess different shapes whether $LiNO_3$ is added or not to the system. While three semi-circles are observed in OPC-0.36 and OPC-0.8 plots, only one is clearly seen when $LiNO_3$ is added to the system. According to Delpech *et al.* [3], the Nyquist plot of aluminium corroding in cement paste consists of one impedance at high frequencies corresponding to the cement paste contribution, followed by a second impedance at low and intermediate frequencies, corresponding to the corrosion process (e.g. oxidation of aluminium and reduction of water). In that work [3], the Nyquist plots were similar to the ones recorded for OPC-0.36 and OPC-0.8. The difference observed for samples OPC-0.36Li and OPC-0.8Li could be correlated with the inhibition of the corrosion by the formation of an Al-Li protective layer at the surface of the metallic aluminium [18]. The impedance induced by the cement paste is then limited because aluminium corrosion is mainly caused by diffusion of OH^- and $Al(OH)_4^-$ [34] inside the interface layer between the aluminium and the cement paste (e.g. the protective Al-Li layer and the corrosion product layer). The Bode plots also revealed that the corrosion occurred in the frequency range 100 mHz – 1 kHz for all samples.

The EIS measurements of the bare aluminium sample in $Ca(OH)_2$ solution is also presented in Figure 2 (see Nyquist and Bode plots on the top row). The shape of the Nyquist plots is similar to the one obtained for aluminium embedded in OPC, while the impedance is smaller revealing a faster corrosion rate, as expected.

To gain information on the corrosion rate of aluminium in the different systems, the corrosion current density (i_{corr}; $\mu A \cdot cm^{-2}$) needs to be calculated, using Equation 1:

$$i_{corr} = \frac{B}{R_t} \qquad \text{(Equation 1)}$$

where R_t is the charge transfer resistance (Ω), assessed by fitting the EIS curves (full lines in Figure 2) using the equivalent electrical circuit (Figure 1) and B is the Stearn-Geary constant (V).

Because the value of B corresponding to the system Al/OPC was not known from the literature, this parameter was determined experimentally using Equation 2:

$$B = \frac{(\beta_a \beta_c)}{2.303\ (\beta_a + \beta_c)} \qquad \text{(Equation 2)}$$

where β_a and β_c are the anodic and cathodic Tafel slopes (V/dec), respectively. The Tafel slopes where determined from the slopes of the anodic and cathodic branches of the polarisation curves. Because in the Tafel extrapolation method, the tested electrode is polarised about 250 mV on either side of the open-circuit potential, the system could be damaged. Therefore, this analysis was performed only once at the end of the test (after ~100 days in this study). Tafel slopes were similar whatever the cement paste composition. Therefore, the Stearn-Geary constant was averaged from all tests in this study. For bare aluminium in $Ca(OH)_2$ solution, Tafel slopes and B were slightly different. All results are given in Table 2.

After determining R_t and B, the corrosion rate was calculated using Equation 3, according to the ASTM procedure G102-89.

$$C_{rate} = 3.27 \times \frac{i_{corr}}{\rho} \times EW \qquad \text{Equation 3}$$

where C_{rate} is the corrosion rate ($\mu m \cdot y^{-1}$), i_{corr} is the corrosion current density ($\mu A \cdot cm^{-2}$), ρ is the density (2.7 $g \cdot cm^{-3}$ for Al) and EW is the equivalent weight (9 $g \cdot equivalent^{-1}$ for Al).

Figure 4 shows the evolution of the corrosion rate in function of time for the different samples studied in this research. As already mentioned elsewhere [9,11,35,36], the corrosion rate decreases with time for all studied systems and reaches a steady state after ~20 days. This also confirms the trend obtained from the evaluation of the EIS measurements.

For the bare aluminium samples immersed in saturated $Ca(OH)_2$ solution, the initial corrosion rate was close to 300 $\mu m \cdot y^{-1}$. Then, it decreases rapidly to reach a steady state around 70 $\mu m \cdot y^{-1}$ after only 4-5 days. It has to be noted that only the first 20 days were recorded for this system. For the aluminium samples embedded in OPC paste matrices, the corrosion rates initially ranged from 10 to 324 $\mu m \cdot y^{-1}$. These rates are slower than the ones already reported (between 1000 and 22000 $\mu m \cdot y^{-1}$) [35,36]. However, in this research, the initial corrosion rate was taken only after 4 days and the corrosion rate could already have decreased during the first days of the tests. Moreover, the tests are performed in absence of oxygen, which is known to increase the aluminium corrosion rate [37]. The smallest initial rate was recorded for OPC-0.36Li and the highest for OPC-0.8 (Figure 4 and Table 3). These results show that combining a cement paste with a low porosity and the addition of $LiNO_3$ as a corrosion inhibitor greatly decrease the initial corrosion rate of aluminium. The other systems gave intermediate corrosion rates with OPC-0.36 corroding slower than OPC-0.8Li. Therefore, the decrease of the initial corrosion rate is more favoured by the decrease of the cement paste porosity than by the addition of a corrosion inhibitor. This could mainly be due to a hampered mass transfer

(water and corrosion products) through the lower porosity of the cement paste. The lower amount of water initially present in the cement paste could also influence these results, although the samples were immersed in saturated $Ca(OH)_2$ solution one day after casting the cement pastes. At the opposite, the use of cement paste with a higher porosity without the presence of corrosion inhibitor does not have an influence on the initial corrosion rate as the rate measured on the bare aluminium was similar to the one of OPC-0.8. This means that for OPC-0.8, the corrosion is limited by the diffusion of hydroxide molecules in the corrosion product layer at the surface of the aluminium and not due to mass transfer limitation through the cement paste. After 20 days, the corrosion rates of bare Al and OPC-0.8 are still close, reinforcing the fact that using a cement paste with a high porosity does not hamper the aluminium corrosion. Nevertheless, an analysis of the evolution of the corrosion rate of bare Al on a longer term is needed to confirm this hypothesis.

At the end of the experiment, after ~100 days, the lowest corrosion rate was still measured for OPC-0.36Li. OCP-0.36 and OPC-0.8 possess the highest corrosion rate, while OPC-0.8Li gives intermediate corrosion rate (Figure 4 and Table 3). Therefore, coupling the presence of $LiNO_3$ inhibitor and minimising the porosity of the cement paste still provide the slowest corrosion rate. Unlike the initial rate, the presence of inhibitor in the cement prevails over the smaller porosity at longer term, as OPC-0.8Li possesses a lower corrosion rate than OPC-0.36. This means that the corrosion is limited by the presence of the protective Li-Al layer at the interface aluminium/cement. However, it has to be noted that cracks appeared in samples OPC-0.36 and OPC-0.8 after ~30 days of immersion in saturated $Ca(OH)_2$ solution. This could explain the sharp increase of the corrosion rate of OPC-0.36 in that period. Afterwards, the corrosion rate of both OPC-0.36 and OPC-0.8 are similar, because the water supply at the surface of the aluminium took place through the crack and no longer through the porosity of the cement. More tests need to be performed to try to avoid the appearance of cracks in the cement paste to gain

a better knowledge of the influence of the cement porosity on the corrosion rate of aluminium, when no corrosion inhibitor is added in the cement paste.

The recorded rates are comparable with corrosion rates obtained from the literature in aerobic atmosphere, while it was expected that oxygen would promote the corrosion rate [37]. Therefore, performing tests in anaerobic conditions does not seem to influence greatly the corrosion of aluminium in contact with OPC pastes. Lower corrosion rates in the range 0.1 – 1.3 $\mu m \cdot y^{-1}$ were also reported, but these tests lasted much longer (from 2 to 27 years) [35,36].

3.3.Microstructural characterisation

Scanning Electron Microscopy (SEM) analysis was carried out to study the interface between the aluminium samples and the different cement pastes after ~100 days of immersion in saturated $Ca(OH)_2$ solution.

Figure 5 shows the cross section of the interface aluminium/cement paste for the different samples studied in this research. The addition of $LiNO_3$ to the OPC pastes resulted in the formation of much thinner corrosion product layers whatever the w/c ratio, confirming the significant effect of the corrosion inhibition. Table 4 gives the corrosion product layer thickness measured for all systems. From these values, the corresponding corrosion rate was calculated and compared to the values obtained by EIS. For all studied systems, the corrosion rate calculated from the SEM pictures is higher than the one obtained from the EIS measurements, mainly for samples without $LiNO_3$ (OPC-0.36 and OPC-0.8), partially due to the lower density of the corrosion products compared to metallic aluminium. However, this hypothesis cannot explain such a big difference and more tests are needed to better understand this phenomenon.

Figure 5 also shows also the presence of holes close to or in contact with the surface of the aluminium samples. Those holes could be due to the formation of the corrosion product layer taking up a much larger volume (because of its lower mass density) than metallic aluminium, leading to stresses in the cement matrix. Hydrogen generation during the corrosion process of aluminium could also have contributed to the creation of internal stresses [9-10]. Needle-like phases are also observed in all samples (only shown for OPC-0.36Li, Figure 5(B)). Those phases are typical from the Ettringite phase but no diffraction analysis was performed to confirm this statement.

The elemental analysis of the interface aluminium/cement paste was also studied by SEM-EDS (Figure 6). For all systems, the corrosion product layer was mainly composed of aluminium and oxygen. Calcium, silicon and other constituents of the cement, were not measured in this corrosion product layer. They were only detected in the cement region. However, point EDS measurements (not shown in the figure) revealed that the cement near the corrosion product layer was enriched in aluminium. This suggests that during the growth of the aluminium oxide, the corrosion product layer is pressed against the cement, allowing aluminium to infiltrate the cement through porosity. However, it was not possible, within this study, to determine whether the larger porosity of the OPC-0.8 and OPC-0.8Li cement pastes allows a deeper penetration of aluminium in the cement. On the other hand, calcium and other constituents of the cement are not diffusing into the aluminium oxide layer, at least during the duration of these tests. More tests are necessary to study the interface between the cement and the corrosion product layer as well as the stresses induced in the cement during aluminium corrosion in more detail.

4. Conclusions

The corrosion of pure aluminium in contact with OPC immersed in saturated $Ca(OH)_2$ solution was studied under anaerobic conditions to mimic the long term geological disposal conditions. The effect of the porosity/mass transfer limitation (by using cement pastes with different w/c ratios) and the addition of $LiNO_3$ (used as corrosion inhibitor) were evaluated. EIS measurements showed that, for all conditions, the corrosion rates were maximal at the beginning of the test and decreased with time up to reach a steady state after a few days.

Initially, the use of a cement paste possessing a lower water-to-cement ratio, and therefore a lower porosity, allows a lower corrosion rate. This is maybe due to the initially lower amount of water present inside the cement and to the more difficult mass transfer (water and corrosion products) through this cement paste with lower porosity. Moreover, the presence of $LiNO_3$ as corrosion inhibitor (OPC-0.36Li) enhances the smaller corrosion rate. By contrast to short term corrosion rate, the presence of inhibitor in the cement prevails over the smaller porosity at longer term (~100 days in this study), as OPC-0.8Li possesses a lower corrosion rate than OPC-0.36. This means that the corrosion is limited by the presence of the protective Li-Al layer at the interface aluminium/cement. Some cracks were also formed in the cement pastes without $LiNO_3$ due to the higher corrosion rate, producing extra corrosion products and hydrogen gas, leading to stresses in the encapsulation matrix.

SEM-EDS analysis was realised to look at the interface between the aluminium samples and the cement pastes after ~100 days of corrosion. The corrosion product layer thicknesses are the smallest for OPC-0.36Li (~10 µm) and OPC-0.8Li (~25 µm), while they increase to ~160 and ~100 µm for OPC-0.36 and OPC-0.8, respectively. These results revealed that the corrosion product layer thicknesses are higher than the one expected from EIS measurements. An elemental analysis of the interface revealed that the corrosion product layer is composed exclusively of aluminium and oxygen, while the cement paste close to this corrosion product layer is enriched in aluminium. This suggests that during the growth of the aluminium oxide,

the corrosion product layer is pressed against the cement, allowing aluminium to infiltrate the cement through porosity, without any diffusion of cement element through this corrosion product layer.

5. Acknowledgment

The research leading to these results has received funding from the “Technical Passive project” and was also performed in the broader framework of a public-public cooperation between ONDRAF/NIRAS and SCK CEN. However, the proposed approach and obtained results in no way entail a decision of ONDRAF/NIRAS whatsoever on this approach as a solution for the long-term management of this waste.

The authors acknowledge also Pieter Schroeders, Steven Smets, Sabrina Lunardi, Stef Geukens and Wim Verwimp for the technical support and Anne-Marie De Wilde for her assistance with the MIP measurements.

References

[1] A. Leenaers, C. Detavernier, S. Van den Berghe, *J. Nucl. Mater.* 2008, *381*, 242.

[2] Y. S. Kim, H. T. Chae, S. Van den Berghe, A. Leenaers, V. Kuzminov, *J. Nucl. Mater.* 2020, *529*, 151926.

[3] S. Delpech, C. Cannes, N. Barré, Q. T. Tran, C. Sanchez, H. Lahalle, D. Lambertin, S. Gauffinet, C. Cau-dit-Coumes, *J. Electrochem. Soc.* 2017, *164*, C717.

[4] E. Deltombe, M. Pourbaix, *Corrosion* 1958, *14*, 16.

[5] H. G. Godard, *Mater. Performance* 1981, *20*, 9.

[6] H. Mansour, F. M. El-cheikh, H. M. Moustafa, A. El-wafa, *Trans. of the SAEST* 1992, *27*, 25.

[7] M. R. Tabrizi, S. B. Lyon, G. E. Thompson, J. M. Ferguson, *Corros. Sci.* 1991, *32*, 733.

[8] J. Zhang, M. Klasky, B. C. Letellier, *J. Nucl. Mater.* 2009, *384*, 175.

[9] C. Mendibide, V. Dusquesnes, V. Deydier, X. Bourbon, D. Crusset, *Mater. Corros.* 2020, *72*, 1.

[10] A. Setiadi, N. B. Milestone, J. Hill, M. Hayes, *Adv. Appl. Ceram.* 2006, *105*, 191.

[11] H. Kinoshita, P. Swift, C. Utton, B. Carro-Mateo, G. Marchand, N. Collier, N. Milestone, *Cement Concrete Res.* 2013, *50*, 11.

[12] M. A. Chavda, H. Kinoshita, J. L. Provis, *Adv. Appl. Ceram.* 2014, *113*, 453.

[13] N. C. Collier, N. B. Milestone, P. D. Swift, *Adv. Appl. Ceram.* 2010, *109*, 269.

[14] N. C. Collier, N. B. Milestone, L. E. Gordon, S. C. Ko, *J. Nucl. Mater.* 2014, *452*, 457.

[15] C. Cau-dit-Coumes, D. Lambertin, H. Lahalle, P. Antonucci, C. Cannes, S. Delpech, *J. Nucl. Mater*. 2014, *453*, 31.

[16] U. Nürnberger, *Otto-Graf-Journal* 2001, *12*, 69.

[17] T. Matsuo, M. Matsuda, M. Hironaga, Y. Horikawa, *J. Nucl. Sci. Technol.* 1996, *33*, 852.

[18] T. Matsuo, T. Izumida, M. Hironaga, Y. Horikawa, T. Shiomi, *J. Nucl. Sci. Technol.* 1997, *34*, 823.

[19] T. Matsuo, T. Nishi, M. Matsuda, T. Izumida, *J. Nucl. Sci. Technol.* 1995, *32*, 912.

[20] M. Nicu, L. Ionascu, C. Turcanu, F. Dragolici, *Rom. J. Phys.* 2015, *60*, 1193.

[21] R. G. Kelly, J. R. Scully, D. W. Shoesmith, R. G. Buchheit, *Electrochemical techniques in corrosion science and engineering*, Marcel Dekker, Inc., New York 2003.

[22] E. E. Stansbury, R. A. Buchanan, *Fundamentals of electrochemical corrosion*, ASM International, Material Park, Ohia 2000.

[23] G. Song, *Cement Concrete Res.* 2000, *30*, 1723.

[24] M. Cabeza, P. Merino, A. Miranda, X. R. Nóvoa, I. Sanchez, *Cement Concrete Res.* 2002, *32*, 881.

[25] J. M. Cruz, I. C. Fita, L. Soriano, J. Payá, M. V. Borrachero, *Cement Concrete Res.* 2013, *50*, 51.

[26] L. Fan, H. Lu, J. Leng, Z. Sun, C. Chen, *J. Electrochem. Soc.* 2016, *163*, A8.

[27] J. Wysocka, M. Cieslik, S. Krakowiak, J. Ryl, *Electrochim. Acta* 2018, *289*, 175.

[28] H. Zhao, J. Ding, Y. Huang, Y. Tang, W. Xu, D. Huang, *Struct. Concrete* 2019, *20*, 1750.

[29] C. Andrade, M. Keddam, X. R. Nóvoa, M. C. Pérez, C.M. Rangel, H. Takenouti, *Electrochim. Acta* 2001, *46*, 3905.

[30] M. Criado, D. M. Bastidas, S. Fajardo, A. Fernández-Jiménez, J. M. Bastidas, *Cement Concrete Comp.* 2011, *33*, 644.

[31] M. A. Ismail, M. Ohtsu, *Constr. Build. Mater.* 2006, *20*, 458.

[32] G. Trabanelli, C. Monticelli, V. Grassi, A. Frignani, *Cement Concrete Res.* 2005, *35*, 1804.

[33] W. Wang, H. Chen, X. Li, Z. Zhu, *Constr. Build. Mater.* 2017, *143*, 289.

[34] D. Chu, R. F. Savinell, *Electrochim. Acta* 1991, *36*, 1631.

[35] D. J. Lee, C. R. Wilding, *Report CPDG(89)P263*, 1989.

[36] C. J. Walton, F. L. McGeary, E. T. Englehart, *Corrosion* 1957, *13*, 41.

[37] L. Hao, J. Dai, Z. Huang, C. Lei, F. Zheng, J. Li, Y. Fan, S. Wang, *Int. J. Electrochem. Sc.* 2021, *16*, 210529.

Figures

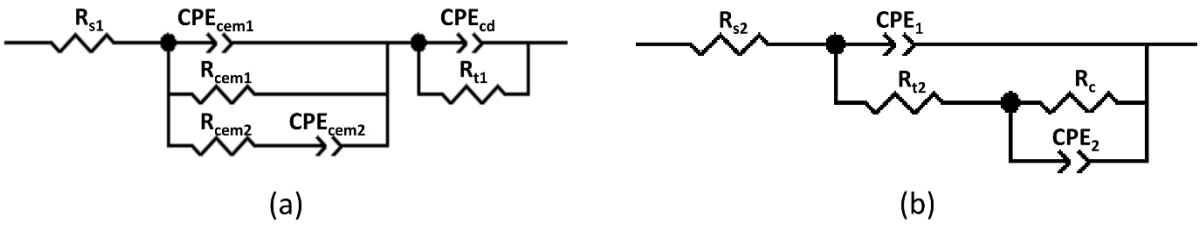

Figure 1. Schematic representation of the equivalent electrical circuits used in this study for (a) the aluminium/cement corroding system; (b) the bare aluminium/Ca(OH)2 corroding system.

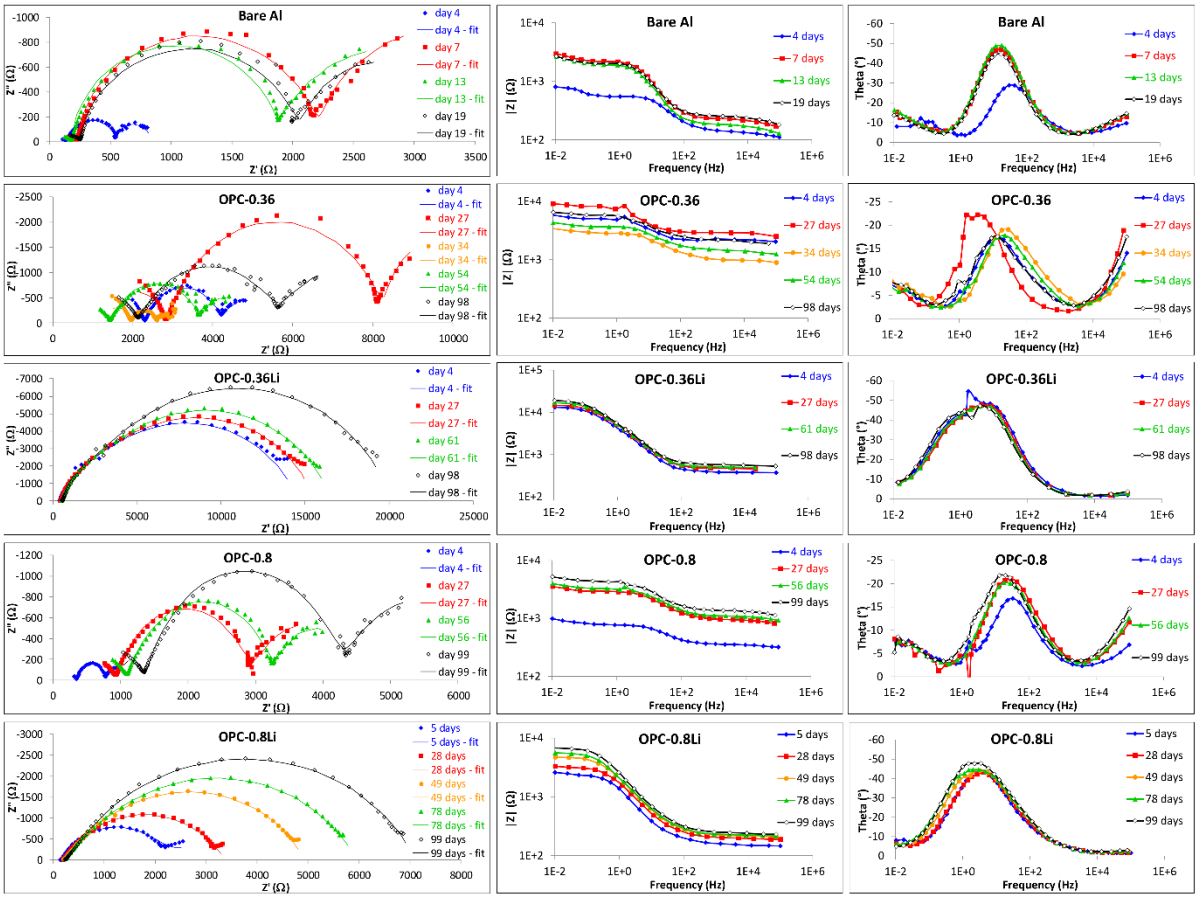

Figure 2. EIS spectra (Nyquist and Bode plots) obtained for bare aluminium, OPC-0.36, OPC-0.36Li, OPC-0.8 and OPC-0.8Li in function of time, when immersed in a saturated $Ca(OH)_2$ solution.

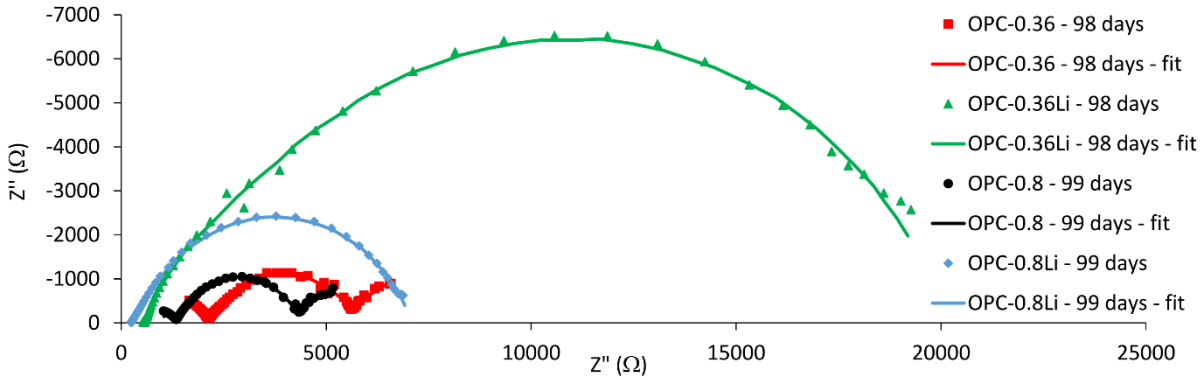

Figure 3. Comparison of the Nyquist plots obtained for OPC-0.36, OPC-0.36Li, OPC-0.8 and OPC-0.8Li at the end of the test (98 or 99 days).

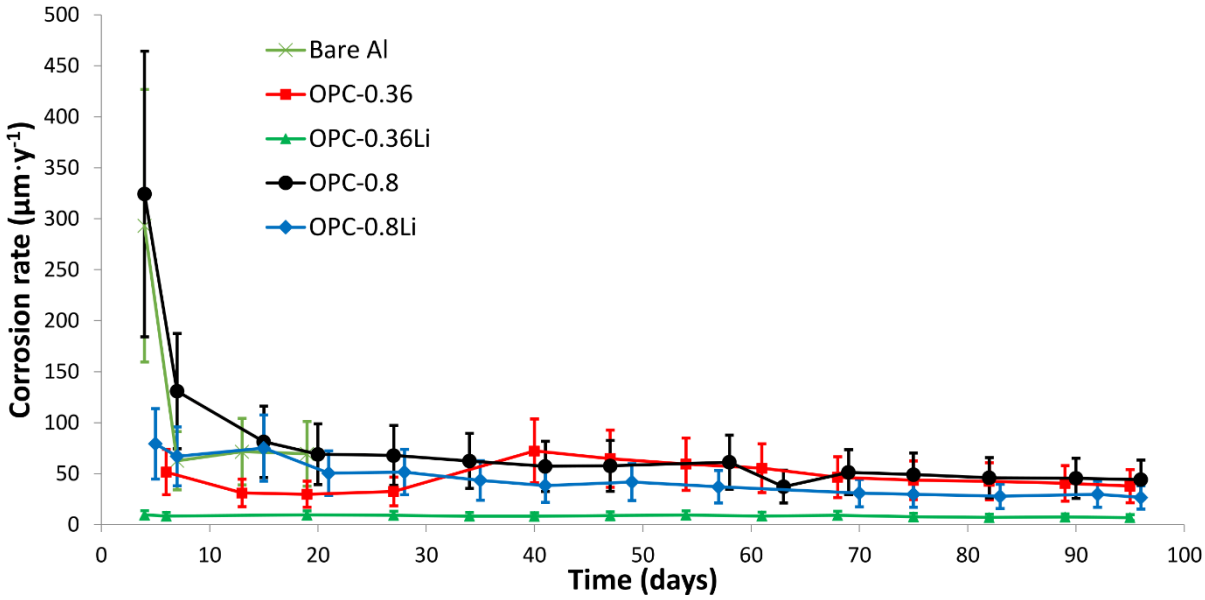

Figure 4. Evolution of the corrosion rate of bare Al immersed in sat. $Ca(OH)_2$ and Al embedded in different OPC cement pastes (and immersed in sat. $Ca(OH)_2$ solution).

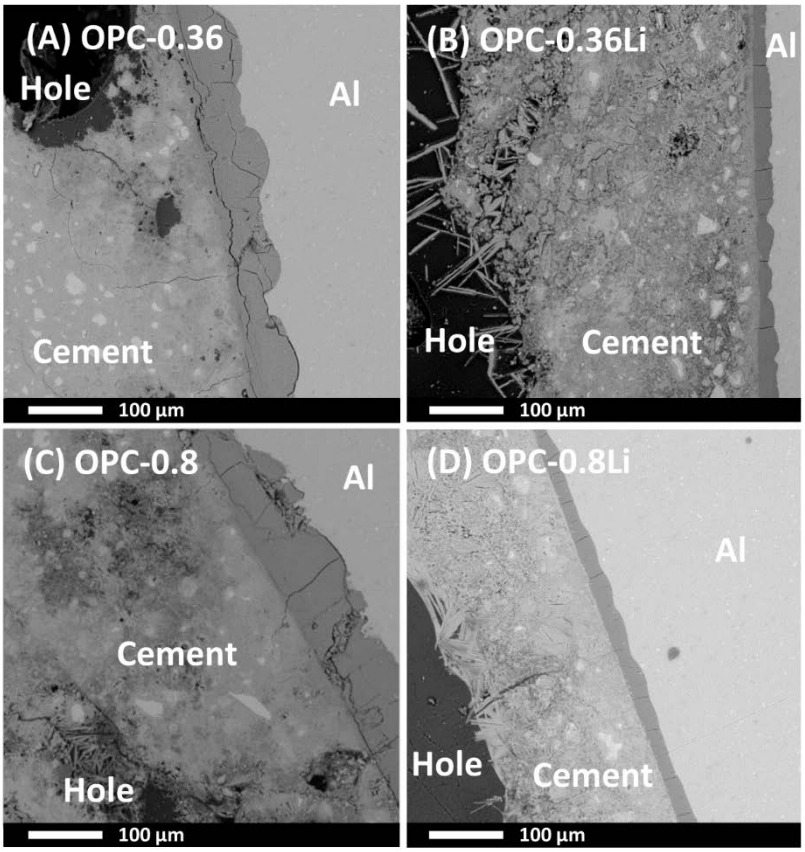

Figure 5. SEM micrographs of the cross sections at the interface aluminium/cement paste for (A) OPC-0.36, (B) OPC-0.36Li, (C) OPC-0.8 and (D) OPC-0.8Li.

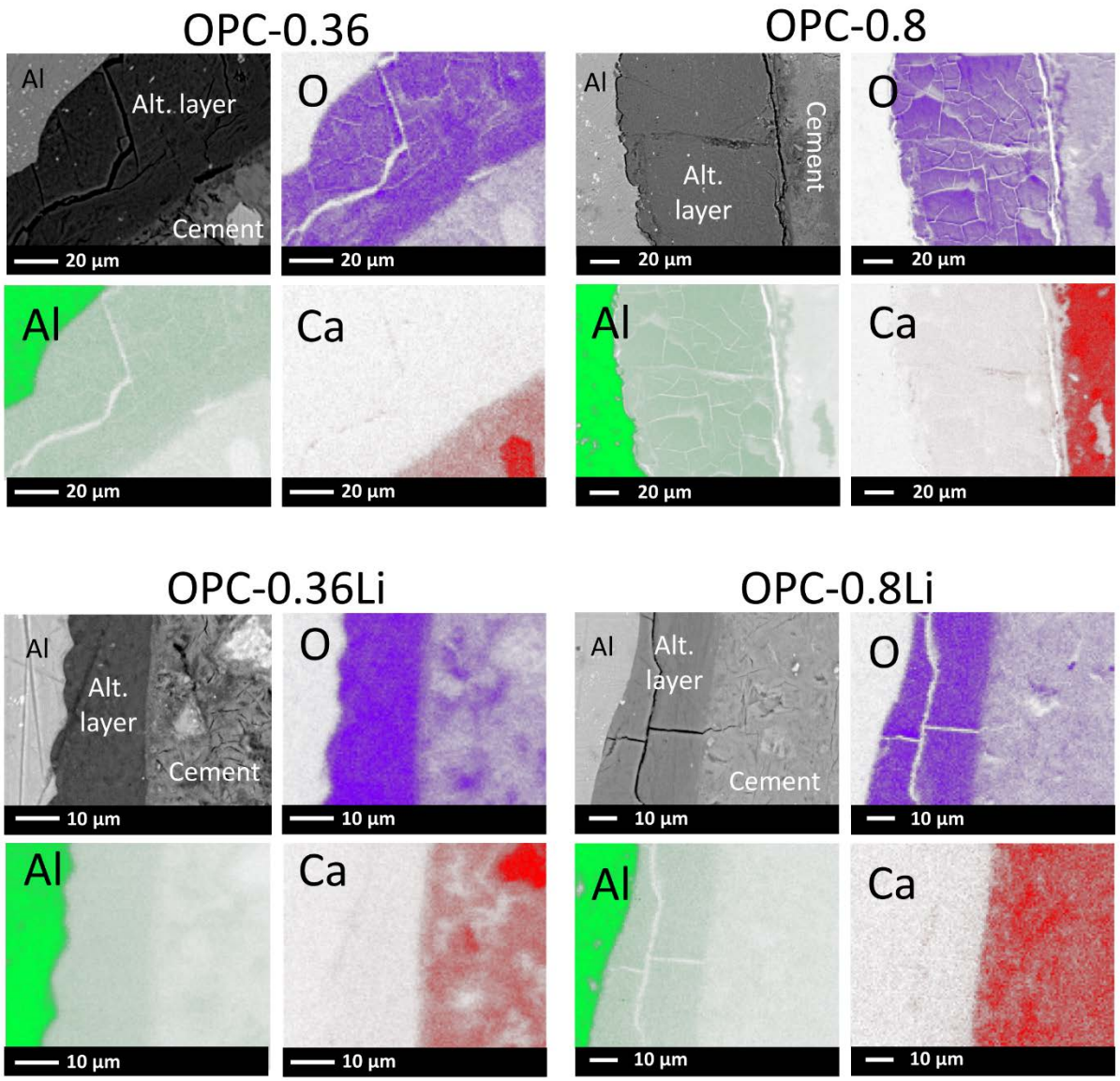

Figure 6. Elemental mapping of the interface aluminium/cement for OPC-0.36, OPC-0.36Li, OPC-0.8 and OPC-0.8Li.

Tables

Table 1. Average pore radius and percentage of porosity of the four different OPC cement pastes.

Cement	OPC-0.36	OPC-0.36Li	OPC-0.8	OPC-0.8Li
Average pore radius (nm)	10.7	10.1	31.6	38.8
Porosity (%)	10.0	7.1	30.4	30.3

Table 2. Tafel slopes and Stern-Geary constant determined experimentally.

Samples	β_a (V/dec)	β_c (V/dec)	B (V)
Al in OPC	0.118	0.194	0.032
Bare Al	0.106	0.202	0.030

Table 3. Initial and final corrosion rate.

Samples	Initial corrosion rate ($\mu m \cdot y^{-1}$)	Final corrosion rate (after ~100 days; $\mu m \cdot y^{-1}$)
Bare Al	293 ± 134	69 ± 32[a]
OPC-0.36	52 ± 22	38 ± 16
OPC-0.36Li	10 ± 4	7 ± 3
OPC-0.8	324 ± 140	44 ± 19
OPC-0.8Li	79 ± 34	27 ± 12

[a] After only 20 days.

Table 4. Comparison between the alteration layer thickness observed by SEM and calculated from EIS analysis.

Samples	Corrosion product layer thickness (SEM) (µm)	Mean corrosion product layer thickness (SEM) (µm)	Estimated corrosion rate (SEM) ($\mu m \cdot y^{-1}$)	Calculated corrosion product layer thickness (EIS) (µm)[a]	Calculated corrosion rate (EIS) ($\mu m \cdot y^{-1}$)[a]
OPC-0.36	27 – 450	160	61	12.6 ± 5.7	48.4 ± 22.1
OPC-0.36Li	5 – 40	10	38	2.2 ± 1.0	8.5 ± 3.7
OPC-0.8	55 – 250	100	380	18.5 ± 8.0	70.4 ± 30.4
OPC-0.8Li	15 – 40	25	95	11.2 ± 5.0	42.5 ± 19.0

[a] Obtained from the integration of the curves presented in Figure 4.

Graphical abstract + text (max 70 words)

The corrosion rate of aluminium in contact with Ordinary Portland Cement in anaerobic conditions was evaluated by Electrochemical Impedance Spectroscopy and Scanning Electron Microscopy. The use of both corrosion inhibiting agent ($LiNO_3$) and low porosity cement paste allow a sensible decrease of the corrosion rate. Initially, the lower porosity favoured lower corrosion rates, while at longer term (~3 months) the addition of $LiNO_3$ seems to control the lower corrosion rates.